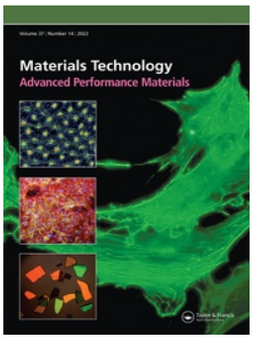

Taylor & Francis
Taylor & Francis Group

Materials Technology
Advanced Performance Materials

ISSN: 1066-7857 (Print) 1753-5557 (Online) Journal homepage: www.tandfonline.com/journals/ymte20

Biocompatibility vs antibacterial activity: chitosan-mediated nanosilver/PCL/gelatin nanofibers

Dilshan Chandraguptha, Lochana Fernando, Lalinka Herath, V. Umayangana Godakanda, Nirmal Perera, Sameera Samarakoon, K. M. Nalin de Silva, Gareth R. Williams & W. Rohini M. de Silva

To cite this article: Dilshan Chandraguptha, Lochana Fernando, Lalinka Herath, V. Umayangana Godakanda, Nirmal Perera, Sameera Samarakoon, K. M. Nalin de Silva, Gareth R. Williams & W. Rohini M. de Silva (2026) Biocompatibility vs antibacterial activity: chitosan-mediated nanosilver/PCL/gelatin nanofibers, Materials Technology, 41:1, 2605316, DOI: 10.1080/10667857.2025.2605316

To link to this article: https://doi.org/10.1080/10667857.2025.2605316

MATERIALS TECHNOLOGY
2026, VOL. 41, NO. 1, 2605316
https://doi.org/10.1080/10667857.2025.2605316

Taylor & Francis
Taylor & Francis Group

RESEARCH ARTICLE

OPEN ACCESS Check for updates

Biocompatibility vs antibacterial activity: chitosan-mediated nanosilver/PCL/gelatin nanofibers

Dilshan Chandraguptha[a], Lochana Fernando[a,b], Lalinka Herath[a,c], V. Umayangana Godakanda[a], Nirmal Perera[d], Sameera Samarakoon[d], K. M. Nalin de Silva[a], Gareth R. Williams[e] and W. Rohini M. de Silva[a,c]

[a]Center for Advanced Materials and Devices (CAMD), Department of Chemistry, Faculty of Science, University of Colombo, Colombo, Sri Lanka; [b]Faculty of Humanities and Sciences, Sri Lanka Institute of Information Technology, Malabe, Sri Lanka; [c]Department of Biomedical Science, Faculty of Science, NSBM Green University, Homagama, Sri Lanka; [d]Institute of Biochemistry, Molecular Biology and Biochemistry (IBMBB), University of Colombo, Colombo, Sri Lanka; [e]UCL School of Pharmacy, University College London, London, UK

ABSTRACT

Electrospinning is an efficient approach to prepare nanofiber scaffolds that mimic local tissue environments. While many reported scaffolds incorporate nanoparticles, detailed assessments of how nanosilver distribution affects antibacterial activity and biocompatibility remain limited. In this study, we developed an electrospun biopolymer scaffold composed of polycaprolactone and gelatin with chitosan-mediated nanosilver (C-AgNPs), introduced either by bulk surface coating or by dispersing the NPs within the electrospinning solution. The C-AgNP surface-coated scaffold exhibited antibacterial activity against *Staphylococcus aureus* and *Escherichia coli*, whereas the dispersed scaffold did not. However, the dispersed scaffold promoted higher dermal fibroblast viability (82.7%) compared with the coated scaffold (60.9%). Zebrafish embryo assays further revealed mild developmental toxicity from the coated scaffold but no observable toxicity from the dispersed formulation. These findings demonstrate a distinct trade-off between antibacterial efficacy and cytocompatibility depending on nanoparticle distribution. Understanding this relationship is critical for designing electrospun nanofiber scaffolds with balanced biological properties.

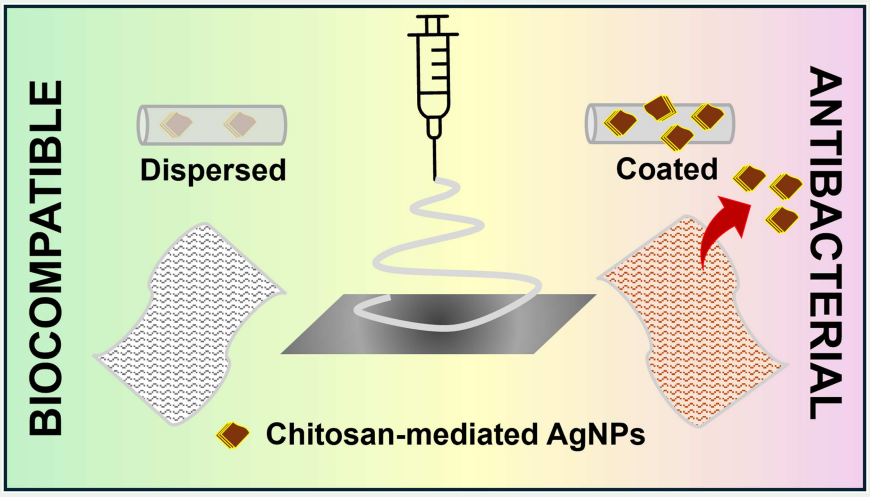

ARTICLE HISTORY
Received 22 April 2025
Accepted 10 December 2025

KEYWORDS
Electrospun nanofibers; nanosilver; antibacterial activity; wound healing

CONTACT Gareth R. Williams g.williams@ucl.ac.uk UCL School of Pharmacy, University College London, 29-39 Brunswick Square, London, WC1N, 1AX, UK; W. Rohini M. de Silva rohini@chem.cmb.ac.lk Center for Advanced Materials and Devices (CAMD), Department of Chemistry, University of Colombo, Colombo, 00300, Sri Lanka

Supplemental data for this article can be accessed online at https://doi.org/10.1080/10667857.2025.2605316.

Introduction

Electrospun nanofibers have been widely explored over the past two decades because they can exhibit excellent properties addressing the long-lasting problem of human tissue damage. Tissue engineering employs an initial framework (scaffold), on which cells multiply and grow to fully functionalized tissues. With the natural blood supply being established, the scaffold disintegrates, allowing the new tissues to merge with their surroundings [1]. The existing literature reports a variety of polymer-based electrospun nanofibers with potential uses in tissue engineering, with systems to support human skin being particularly extensively exploited [2]. The synthetic polymer polycaprolactone (PCL) has been extensively studied for fibre generation due to its high mechanical strength and ease of electrospinning [3,4]. PCL is often combined with biopolymers such as gelatin (Gel) [5], chitosan [6], alginate [7], etc., to give the scaffold favourable properties that foster cell proliferation and differentiation [8].

In recent years, focus has arisen on using metal nanoparticles such as nanosilver (AgNPs) in nanofibers to bestow antibacterial activity in tissue engineering scaffolds, with the goal of preventing infection [9,10]. The direct application of silver (Ag) to accelerate wound healing dates back to 18th-century Egypt [11]. Despite being highly active against various pathogenic microorganisms, Ag has considerable toxicity due to its accumulation in lysosomes and induction of apoptosis mechanisms [12]. However, using AgNPs in place of larger particles can overcome the toxicity of Ag to a significant extent [13]. A variety of physicochemical [14] and biomimetic methods can be used to synthesise AgNPs, with biomimetic or 'green-synthesis' methods felt particularly appropriate for tissue engineering purposes as they avoid the use of potentially toxic chemicals. In that context, the use of chitosan in developing AgNPs has gained attention. Chitosan originates from chitin, which is accumulated in massive amounts in crustacean wastes [15]. Chitosan has active hydroxyl and amino functional groups that can provide chelating effects and antimicrobial activity [16]. The polymer itself is known to be highly biocompatible, and the toxicity of chitosan-mediated nanosilver (C-AgNP) has been assessed using standard toxicity assessments [17].

Various studies have explored AgNPs and their nanocomposites in a range of polymer-based nanofibers [9]. One study showed that higher concentrations (100–400 μg/mL) of AgNPs show greater antibacterial activity; however, there was also significant cytotoxicity when the NPs were incorporated in a polylactic acid (PLA) and chitosan electrospun system by drop coating [18]. Another study explored Ag_2S NPs in PCL-based electrospun fibres, showing antibacterial activity and tissue regeneration responses [19]. Recent work has also been conducted to evaluate the effectiveness of PCL/chitosan [20], PCL/collagen [21] and PCL/poly(methyl methacrylate)/polyglycerol sebacate (PGS) [22] electrospun nanofibers coated with AgNPs.

Nevertheless, there is no comprehensive analysis of how the nanosilver incorporation in nanofibers affects antibacterial activity, cell viability and biocompatibility. In this study, we used newly synthesised and characterised C-AgNPs (previously reported to have low toxicity) and introduced them to electrospun fibres either by bulk surface coating or blending [15]. We also observed the effect of washing and heating coated C-AgNPs. The results showed that the two methods of C-AgNP incorporation differently affect antibacterial activity and cell viability. This was determined using bacterial studies, cell proliferation assays [23,24] and zebrafish embryonic model toxicity tests (approximately 70% of human genes have at least one obvious zebrafish orthologue) [25]. This study can help us understand the effect of C-AgNP distribution in PCL/Gel nanofibers, which is beneficial in designing state-of-the-art electrospun scaffolds balancing the toxicity and antibacterial effects of nanoparticles for tissue engineering.

Materials and methods

Chemical reagents

Silver nitrate (extra pure AR), chitosan (low MW, extra pure), chloroform (extra pure AR) and gelatin powder for bacteriology were purchased from Srichem. Sodium hydroxide pellets GPR were purchased from Park Scientific, and ciprofloxacin antibiotic discs (CIP 5 μg) were obtained from Liofilchem. Acetic acid (99.8%), polycaprolactone (PCL; average Mn-80,000 Da), phosphate-buffered saline tablets, trypsin/EDTA, foetal bovine serum (FBS) and Dulbecco's Modified Eagle's medium (DMEM) were purchased from Sigma-Aldrich. Cadmium nitrate tetrahydrate and Muller–Hinton agar were purchased from HIMEDIA. Deionized water was used for all the experiments.

Synthesis of C-AgNPs

First, 0.20 g of chitosan was dissolved in 40.0 mL of 1% acetic acid solution and stirred for 10 minutes at room temperature (27 °C). The obtained chitosan solution was centrifuged at 3000 rpm for 30 minutes, and 3.0 mL of 0.1 mol/dm^3 $AgNO_3$ solution was added to the supernatant. Finally, 100 µL of freshly prepared 1 M NaOH was added and the mixture stirred at 1500 rpm until a persistent yellow-brown colour was obtained [15].

Preparation of electrospinning solutions

Solutions with varying concentrations of PCL and gelatin were prepared, and after initial optimisation, a solution comprising PCL 25% (w/v) and gelatin 2.5% (w/v) in 1:1 v/v chloroform (CF) and 80% aqueous acetic acid solution was selected. Solid C-AgNPs (20 mg) were dispersed in an 80% acetic acid solution by ultrasonication (BIOBASE) until a homogenised mixture was obtained. An equal volume of chloroform was then added. To prepare the fibres with NPs dispersed throughout the matrix, PCL and Gel were finally added to this suspension at concentrations of 25% and 2.5% w/v, respectively. All solutions were prepared by dissolving the polymers in 6.0 mL of solvent mixture and stirred at 1200 rpm for 18 h in closed vessels at 30 °C.

Preparation of electrospun nanofibers and their modifications

All scaffolds were prepared using a monoaxial electrospinning setup at an ambient temperature of 27 °C. The prepared polymer blends for electrospinning were loaded into a syringe (Terumo 5CC) fitted with a spinneret (22 gauge), ensuring no air bubble retention. The tip-to-collector distance was adjusted to 15 cm, and the feeding rate was fixed at 0.5 mL/h, controlled by a syringe pump (KDS100, Cole-Parmer). A high direct-current voltage of 10.0 kV was applied between the spinneret and a flat-plate stationary collector to generate PCL/Gel/C-AgNP(dis) nanofibers. One millilitre of polymer solution was dispensed to prepare each of the nanofiber mats.

To generate coated scaffolds, an area of around 1 cm^2 was cut out from prepared PCL/Gel scaffolds (without C-AgNPs) and immersed in 4.0 mL of a C-AgNP suspension in sterile vials. The vials were shaken at 60 rpm in a shaking incubator (GEMMYCO, Model: IN-666) for 3 h at 30 °C to form PCL/Gel/C-AgNP(coat) scaffolds. The prepared C-AgNP-coated scaffolds were immersed in deionized water (4.0 mL) and shaken under the same conditions to explore the influence of washing. Furthermore, C-AgNP-coated scaffolds were also heated for 3 h at 60 °C to check the effect of heating.

Characterization

A UV-Vis spectrophotometer (Thermo Scientific Genesys 10S UV-Vis 2M1R102202) was used to obtain absorbance readings in the 200–700 nm range for C-AgNPs [26]. The surface morphology of the nanofibers was observed and assessed using a scanning electron microscope (SEM) fitted with an energy-dispersive X-ray (EDX) attachment (Carl Zeiss Evo 18 microscope, accelerating voltage: 10–20 kV, probe current: 1–25 pA). The ImageJ software (version 1.8.0) was used to calculate nanofiber diameters. A powder X-ray diffractometer (Rigako, SmartLab SE) with Cu Kα radiation was employed to collect X-ray diffraction (XRD) patterns at a scan rate of 5° min^{-1} over the range of 5°–80° 2θ. The vibrational bands of the nanofiber scaffolds were observed using a Fourier transform infra-red (FT-IR) spectrophotometer (PerkinElmer Spectrum Two) within the wavenumber range of 400–4000 cm^{-1}. The attenuated transmission (ATR) mode was used with 1 cm^{-1} resolution, averaged from 32 scans.

Antibacterial disk diffusion assay

The antibacterial effects of the C-AgNPs and electrospun fibre scaffolds were determined by the disk diffusion method [27,28]. Briefly, C-AgNPs and all tested scaffolds were screened for their in vitro antibacterial activity against aerobic gram-positive *Staphylococcus aureus* ATCC 27853 and aerobic

gram-negative *Escherichia coli* ATCC 25992. A bacterial inoculum was prepared by subculturing microorganisms on Mueller–Hinton agar (MHA) at 37 °C for 24 h. The bacterial cells were harvested using 5 mL of 0.9% NaCl and diluted to 0.5 McFarland [1.5×10^8 CFU/mL (CFU: colony-forming unit)]. The prepared bacterial inoculum was spread on the agar surface of Petri dishes using a sterilised spreader.

A volume of 10 µL of C-AgNP suspension, chitosan and NaOH solution (blank), chitosan solution, 1% acetic acid solution, positive control (ciprofloxacin 5 µg in 10 µL of deionized water), or negative control (sterile deionized water) was separately added to previously sterilised filter paper disks (diameter: 6 mm). The solution was allowed to dry within a laminar flow hood. Each plate was separated into five parts, and a schematic diagram of the disc arrangement on the agar plate is illustrated in Figure S1a (Supporting Information). Similarly, circular disks of selected fibre scaffolds with a diameter of 6 mm were sterilised under UV light for 30 minutes on each side, in separate zipped locked bags. Subsequently, the sterilised scaffold mats were placed on agar plates with the same positive and negative controls as illustrated in the schematic diagram in Figure S1b. All plates were incubated at 37 °C for 24 h. Following incubation, the diameter of the growth inhibition zone around the samples was measured to visualise the antibacterial action. The experiments were performed in triplicates and results reported as mean ± standard deviation (S.D.).

Cell culture

BJ human skin fibroblast cells (ATCC: CRL-2522) were cultured in Dulbecco's Modified Eagle's Medium (DMEM) containing L-glutamine and supplemented with FBS (10% v/v), and antibiotics (100 U/mL penicillin and 100 µg/mL streptomycin). All cell culture processing was undertaken in a laminar flow hood (Telstar BIO II A). Cells were incubated at 37 °C in a 5% CO_2 incubator (Forma™ Steri-Cycle™) and harvested by trypsinization following 80% confluency.

Cell proliferation assay

The 3-(4,5-dimethylthiazol-2-yl)-2,5-diphenyl tetrazolium bromide) (MTT) assay was used for cell proliferation assessment [29], which was explored in direct contact mode. BJ cells were cultured in 96-well plates (5000 cells/well) and incubated for 24 h at 37 °C to allow their attachment. After 24 h of incubation, the cells were treated with selected 4 mm × 4 mm samples of electrospun scaffolds (three per well) and incubated for another 24 h at 37 °C. The negative control was complete DMEM medium. At the 24-h time-point, the medium was removed, and the cells were gently washed with PBS (phosphate-buffered saline). MTT solution (0.5 mg/mL in PBS) was added to each well and the plate was incubated for another 4 h at 37 °C. Afterward, 100 µL of dimethyl sulfoxide (DMSO) was added to each well to solubilise the grown formazan crystals. The absorbance corresponding to each sample was measured at 570 nm wavelength using a microplate reader (Synergy HT). The percentage of cell viability of the untreated and treated groups was calculated using the formula (treated ÷ control) × 100% [30]. The morphology of the treated cells was captured using an inverted phase-contrast microscope (Olympus CKX41SF, Japan), and the process was repeated three times (three wells) for the selected scaffolds.

Zebrafish embryonic toxicity test

All zebrafish (*Danio rerio*) broodstock maintenance was carried out according to the Organisation for Economic Cooperation and Development (OECD) guideline No. 236 for fish embryo acute toxicity (FET) tests, in the mini-zebrafish facility at the Department of Chemistry, University of Colombo, Sri Lanka [31]. The detailed procedure for zebrafish culture and embryo selection is provided in previous papers [32,33]. In brief, fertilised embryos were collected from overnight breeding rounds and carefully selected using an Olympus BX53 microscope. Fertilised embryos were identified by cleavage of embryos, and embryos with no transparency, coagulated, or damaged embryos were discarded. The embryo toxicity test was immediately initiated after selecting the intact fertilised eggs. Zebrafish embryos were added to a six-well plate (10 embryos per well) containing 5 mL of zebrafish aquatic water with the prepared membranes (three samples of 1 cm × 1 cm per well). Cd (II) solution (effective concentration of 100 µg/mL) and zebrafish

aquatic water were used as positive control and negative controls, respectively. All the treatments were carried out in triplicate at 28.5 °C, 80% relative humidity, and a photoperiod of 14:10 h light:dark cycle. Following treatments, the zebrafish embryos hatched, and the survival percentages were recorded at 24, 48, 72 and 96 h post fertilisation (hpf) time intervals under an Olympus BX53 microscope fitted with a digital camera (6.6 MP Sony CMOS sensor). The heart rate of zebrafish embryos was recorded as beats per minute at 72 hpf in the control and for two scaffold treatments. This was conducted using direct microscopic observation and a stopwatch. Any development abnormalities of the zebrafish embryos, such as yolk sac oedema (YSE), pericardial oedema (PE) and spinal curvature (SC), were observed at 96 hpf using a microscope.

Statistical analysis

The data collected from all experiments were expressed in terms of mean ± standard deviation (SD), and a two-sample t-test was conducted to probe for any significant differences between the two samples considered. All statistical analyses were performed using SPSS version 26 (IBM Corporation, Armonk, NY, U.S.A.).

Results and discussion

Synthesis and identification of cubic phase C-AgNPs

The C-AgNP precursor solution was prepared (Section 3.2) with minimum atmospheric exposure [34]. The reaction mixture changed from initially being colourless to a mustard yellow and finally to yellowish-brown, providing visual evidence for the successful synthesis of AgNPs (Figure 1a). The yellowish-brown colour intensified as time passed and arises due to the surface plasmon resonance (SPR) of AgNPs [35]. The colour change is also supported by adding NaOH, making the solution more basic, giving the observed colour change [36]. Increasing basicity leads to producing smaller AgNPs and obtaining higher antibacterial activity than larger-size ones [37]. A characteristic UV-vis absorbance peak was observed at a wavelength of 426 nm (Figure 1b), which closely agrees with previous literature [15]. The XRD pattern (Figure 1c) of C-AgNP showed sharp peaks at 27.95°, 32.36°, 46.35°, 54.98°, 57.55° and 76.92°, corresponding to the (111), (200), (220), (311), (222) and (420) planes, respectively (Table S1). These results indicate a cubic phase nanosilver (JCPDS file No. 04-0783), with no other peaks of crystalline impurities.

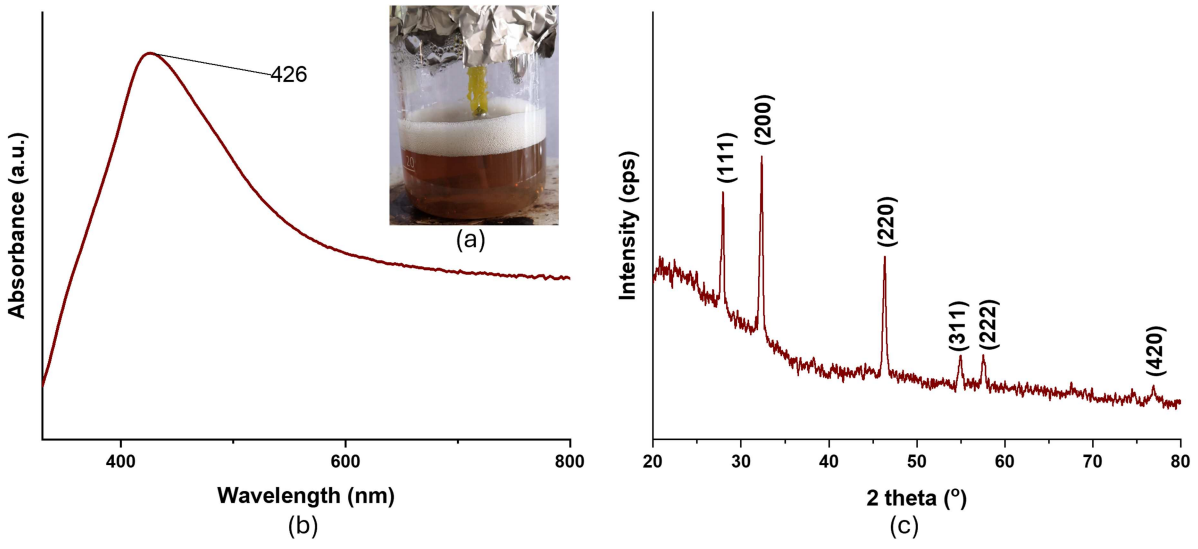

Figure 1. Characterisation of C-AgNPs. (a) Visual identification of a yellowish–brown C-AgNP suspension; (b) UV-vis spectra with 426 nm maximum absorbance; (c) Identification of the cubic phase of C-AgNP by XRD.

Preparation of PCL/gelatin nanofibers

A substantial number of reports exist on the preparation of PCL/Gel electrospun scaffolds, and some have included the incorporation of AgNPs for wound healing and tissue engineering purposes [38]. PCL is a synthetic polymer with good mechanical strength [3], and gelatin is a biopolymer that fosters cell proliferation [39]. Chloroform (CF) [40] was first used to dissolve PCL at a concentration of 25% (w/v) (Table 1).

Electrospinning processing parameters of 15 cm tip-to-collector distance, 1.0 mL/h feeding rate and 10.0 kV operational voltage were optimised to obtain linear PCL fibres with uniform diameters and no bead formation (Figure 2a1 and a2). It was observed that the thickness of the neat PCL fibres was very high; however, due to this, there were fewer spaces among fibres, resulting in less porous fibre mats [26]. A solvent mixture of 1:1 v/v CF and 80% acetic acid [8] was chosen to solubilise both PCL 25% (w/v) and gelatin 2.5% (w/v) in a single blend solution. The electrospun fibres (PCL/Gel) obtained after optimisation showed a notable reduction in nanofiber diameter (622 ± 65 nm), leading to higher porosity (Figure 2b1 and b2). However, the fibres were more non-uniform than the pure PCL formulation, which may be due to the continuous H-bonding between the amine groups of gelatin and the ester groups of PCL [3].

As our next step, the dispersion (dis) method was undertaken by dint of adding solid C-AgNPs in 80% acetic acid solution into the PCL/Gel blend to obtain a homogenous spinnable mixture (Section 3.4). In addition, surface coating (coat) of C-AgNPs onto the neat PCL/Gel scaffold was performed. SEM images reveal that no C-AgNPs were observed on the surface of the fibres in PCL/Gel/C-AgNP(dis) (Figure 2c1 and c2). However, with PCL/Gel/C-AgNP(coat), the presence of some NPs on the fibre exteriors was clear (Figure 2d1 and d2). These observations were verified using EDX (Table 2, Figure S2). A notable Ag content was observed on the scaffold surface-coated with C-AgNPs, whereas only a negligible amount of Ag was detected at the surface of the PCL/Gel/C-AgNP(dis) scaffold. Around a 50% decrease in Ag content was observed after washing the PCL/Gel/C-AgNP(coat) scaffold, showing that a significant amount of C-AgNPs had been washed away. A reduction of Ag concentration was also observed with the PCL/Gel/C-AgNP(coat) scaffold after subjecting it to heat treatment. This latter reduction can be assigned to some of

Table 1. Mean fibre diameters (nm) of electrospun nanofibers.

Scaffolds	Mean fibre diameter ± SD (nm)
PCL	2639 ± 63
PCL/Gel	624 ± 65
PCL/Gel/C-AgNP(dis)	630 ± 45
PCL/Gel/C-AgNP(coat)	846 ± 63

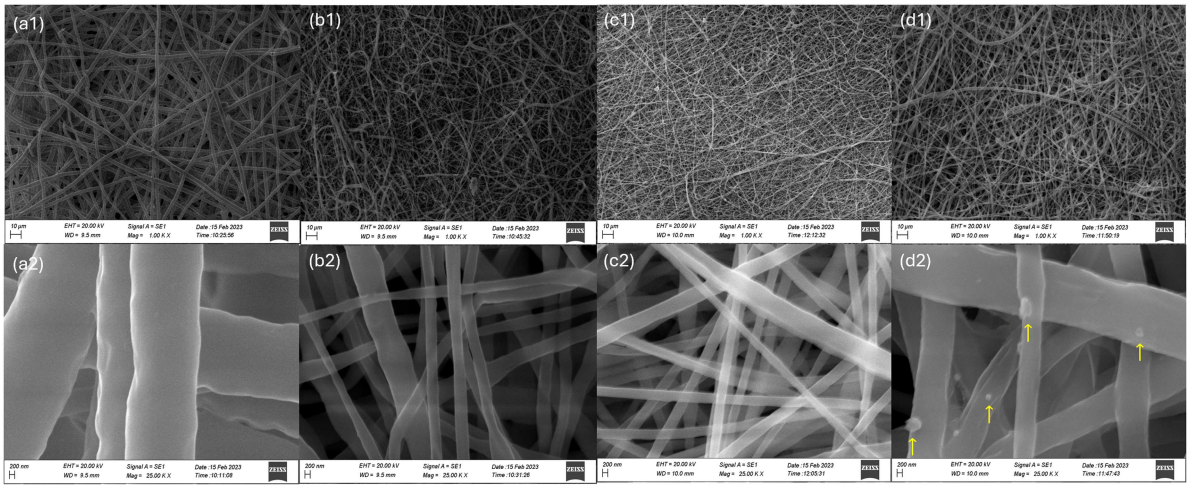

Figure 2. Scanning electron micrographs of electrospun scaffolds: (a1, a2) PCL; (b1, b2) PCL/Gel; (c1, c2) PCL/Gel/C-AgNP (dis); (d1, d2) PCL/Gel/C-AgNP(coat).

Table 2. Summarised EDX results for the electrospun scaffolds' weight (%) of C, O and Ag.

Scaffolds	C	O	Ag
PCL/Gel/C-AgNP(dis)	65.13	34.11	0.09
PCL/Gel/C-AgNP(coat)	64.46	33.57	1.98
PCL/Gel/C-AgNP(coat) -washed	64.95	33.56	0.89
PCL/Gel/C-AgNP(coat) - heated	63.48	35.21	1.06

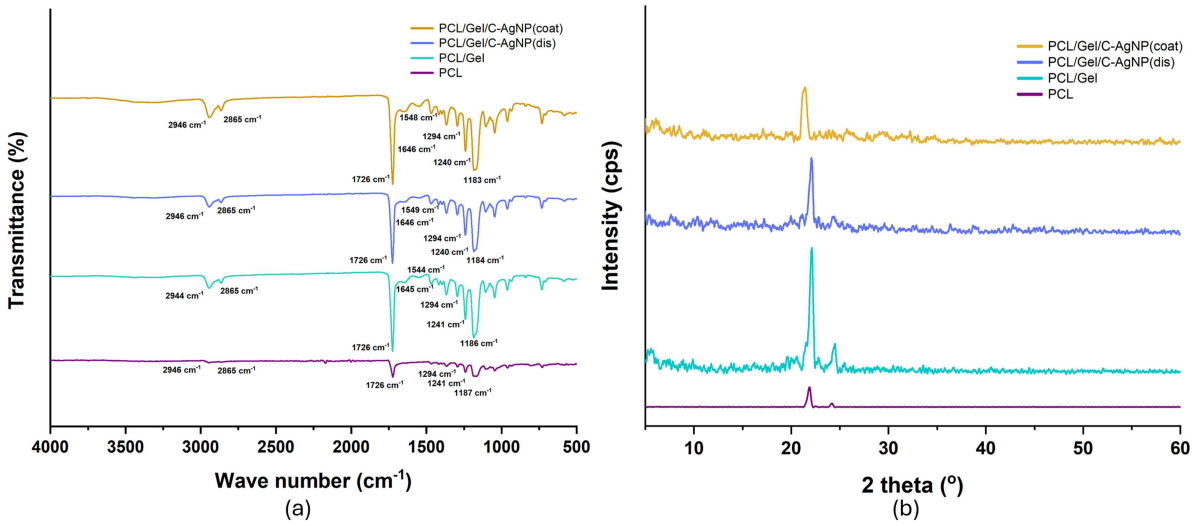

Figure 3. Characterisation of PCL, PCL/Gel, PCL/Gel/C-AgNP(dis) and PCL/Gel/C-AgNP(coat) scaffolds with (a) FT-IR spectra (b) XRD diffraction patterns.

the C-AgNPs becoming submerged within the fibre matrix during the heating process, which took place at approximately the melting temperature of PCL.

FT-IR and XRD analysis of scaffolds

The FT-IR spectra in Figure 3a show the characteristic peaks of PCL, PCL/Gel, PCL/Gel, PCL/Gel/C-AgNP(dis) and PCL/Gel/C-AgNP(coat). The vibrational bands of neat PCL were observed at 2946, 2865, 1726, 1294, 1242 and 1187 cm^{-1}. These bands correspond to —CH_2 stretching, —CH_2 symmetric stretching, C═O stretching, C—C and C—O stretching, C—O—C asymmetric stretching and C—O—C symmetric stretching, respectively [41]. The characteristic peaks of PCL were observed in all the scaffolds, as expected given the majority of the dry mass comprises PCL. With the incorporation of gelatin, characteristic amide peaks at 1645 and 1544 cm^{-1} were observed due to C═O stretching and N—H bending, respectively. A noticeable increase in peak intensity in all scaffolds relative to neat PCL indicates the increased polarity of specific bonds. This can be supported by H-bonding between the amine group of gelatin and the ester group of PCL, as reported earlier [3]. A relatively intense broad peak extending around 3200 to 3500 cm^{-1}, was observed in PCL/Gel and PCL/Gel/C-AgNP(coat) due to O—H stretching, indicating the presence of significant moisture in the developed fibre mats [42].

XRD patterns (Figure 3b) of all scaffolds show two peaks at almost the same 2θ values, characteristic of the Bragg reflections of PCL. These include a high-intensity peak at 21.9° and a lower-intensity peak at 24°. However, a noticeable decrease in the peak intensity of PCL indicates the low crystallinity of PCL nanofibers. The PCL/Gel scaffold exhibits sharp and intense peaks, indicating the high crystallinity of the scaffold. The characteristic peaks obtained for C-AgNPs were not observed in PCL/Gel/C-AgNP(dis) and PCL/Gel/C-AgNP(coat) scaffolds, which may be due to the relatively low content of C-AgNPs in the system. Electrospinning often leads to lowered crystallinity as rapid solvent evaporation allows only a short time before deposition, which is consistent with the observed patterns [43].

Antibacterial disk diffusion assay

The agar disk diffusion assay was carried out to assess the antibacterial activity of synthesised C-AgNPs and all scaffolds: PCL, PCL/Gel/, PCL/Gel/C-AgNP(dis) and PCL/Gel/C-AgNP(coat). The exhibited inhibition zones of C-AgNPs and relevant scaffolds for gram-positive and gram-negative bacterial strains are shown in Figure S3a and S3b. The positive control shows the highest inhibition zones against *Staphylococcus aureus* and *Escherichia coli*, while the negative control has no effect. The results (Table S2) showed that the C-AgNPs are antibacterial against the bacterial strains. Even though chitosan is a known antibacterial agent [16], the results showed no inhibitory zones, which may be due to amount used in synthesis being insufficient to exert a noticeable antibacterial activity. As no inhibitory zones were observed apart from C-AgNPs, the sole antibacterial effect of the nanoparticle was confirmed.

The PCL/Gel/C-AgNP(coat) scaffold gave high antibacterial activity against both bacterial strains, while the PCL/Gel/C-AgNP(dis) scaffold system led to no noticeable effect, as shown in Figure 4 and Table 3. These results suggsted that a silver nanoparticle-coated scaffold system [PCL/Gelatin/C-AgNP(coat)] can quickly release silver ions (Ag^+) from the scaffold matrix. This could have given rise to adherence to or passing of Ag^+ ions through the bacterial cell wall and cytoplasmic membrane to give bacteriostatic or bactericidal activity [44]. However, the antibacterial mechanism of silver nanoparticles is not yet completely understood [45].

The C-AgNPs result in a greater antibacterial effect against gram-negative *Escherichia coli*, with a zone of inhibition of 9.8 ± 1.4 mm compared to 7.5 ± 0.4 mm for gram-positive against *Staphylococcus aureus* (Table S2). This trend was also observed with the coated scaffold system. The action of AgNPs can be described as an electrostatic interaction between the released cationic silver ions and the anionic bacterial cell membrane, followed by permeation and lysis of the cell [46,47]. Our antibacterial results are consistent with other studies that show that a gram-negative bacterium's negative surface charge density is larger than a gram-positive bacterium [48].

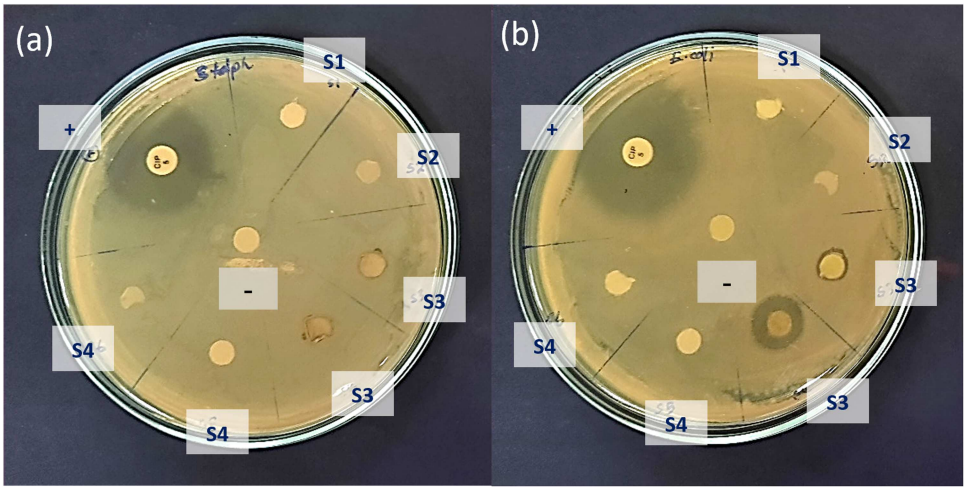

Figure 4. Agar disk diffusion assay for electrospun scaffolds showing inhibition zones against (a) *Staphylococcus aureus* and (b) *Escherichia coli*. (S1) PCL, (S2) PCL/Gel, (S3) PCL/Gel/C-AgNP (coat), (S4) PCL/Gel/C-AgNP (dis), (–) negative control (deionized water) and (+) ciprofloxacin positive control.

Table 3. Diameters of inhibition zones (mm) of agar disk diffusion assay of electrospun scaffolds.

Samples	*Staphylococcus aureus*	*Escherichia coli*
Negative control	0 ± 0	0 ± 0
Positive control	21.0 ± 2.8	29.0 ± 1.4
S1–PCL	0 ± 0	0 ± 0
S2–PCL/Gel	0 ± 0	0 ± 0
S3–PCL/Gel/C-AgNP(coat)	6.5 ± 1.3	8.2 ± 2.1
S4–PCL/Gel/C-AgNP(dis)	0 ± 0	0 ± 0

Cell proliferation assay

To study the inhibitory effects of PCL/Gel, PCL/Gel/C-AgNP(dis) and PCL/Gel/C-AgNP(coat) scaffolds on the proliferation of BJ human skin fibroblast cells, the cells were exposed to the respective scaffold membranes and incubated for 24 h. The results (Table S3) indicated that PCL/Gel/C-AgNP(dis) shows high cell viability with BJ cells (82.7%) compared to PCL/Gel/C-AgNP(coat) (60.9%), with PCL/Gel showing the highest viability (86.5%) (Figure 5). The lower cell viability observed in the coated scaffold [PCL/Gel/C-AgNP(coat)] may be due to the C-AgNP coating on its surface resulting in extensive Ag^+ ion release, leading to uptake into the intercellular microenvironment, potentially hindering fibroblast cell attachment and growth. It is well understood that the physicochemical properties of scaffolds with nanoparticles (e.g. size, shape, composition, surface functionalization and surface hydrophobicity/hydrophilicity) play a key role in manipulating their interactions with cells [49,50]. Therefore, we suggest that this could be the reason for the significantly lower cell viability ($p \leq 0.05$) of PCL/Gel/C-AgNP(coat) compared to both PC/Gel and PCL/Gel/C-AgNP(dis) scaffolds.

Zebrafish embryonic toxicity assay

The practical applicability and the implications of nanofibrous scaffold materials must be studied using animal models to understand biocompatibility with complex tissues. Zebrafish animal models have demonstrated several advantages, such as the ability to study vertebrate developmental biology [51,52], real-time developmental tracking [53,54] and being genetically similar to humans [55]. This makes them a suitable animal model in which to study the effects of scaffold materials [56].

The hatching rate was calculated as the number of hatched embryos from their chorion, divided by the total number of embryos at the time points of 24, 48, 72 and 96 hpf. The calculated zebrafish embryo hatching rates (%) of PCL/Ge/C-AgNP(dis) and PCL/Gel/C-AgNP(coat) treatments are indicated in Figure 6a. It was observed that all the embryos were usually hatched at 96 hpf time points for both the PCL/Gel/C-AgNP(dis) scaffold treatment and the negative control. The PCL/Gel/C-AgNP(coat) scaffold treatment gave a lower 50% hatching rate at 72 and 96 hpf. The significantly lower hatching rates for PCL/Gel/C-AgNP(coat) scaffold can be attributed to the release of Ag^+ that caused additional stress and thus hindered hatching. These results are also consistent with the cell viability tests. The positive control demonstrated the lowest embryo hatching rate, at 3.33% at both 72 and 96 hpf time points.

When considering the survival rate of zebrafish embryos (Figure 6b), the positive control showed time-dependent embryonic toxicity even after 24 hpf while demonstrating a 100% motility rate at the 96 hpf

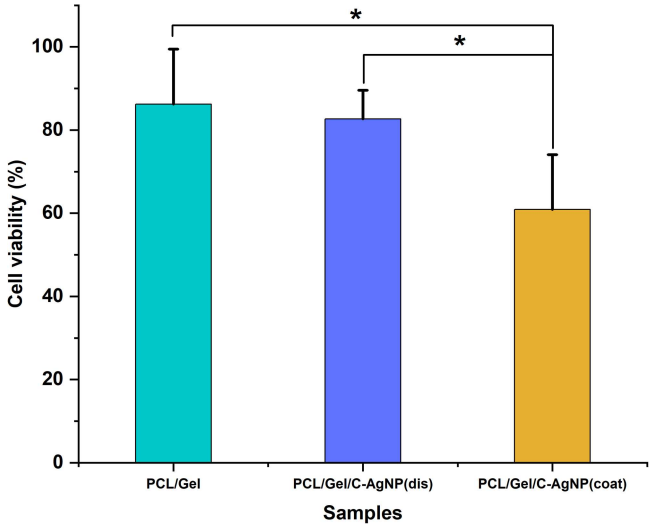

Figure 5. Cell viability at 24-h time point of PCL/Gel (86.5%), PCL/Gel/C-AgNP(dis) (82.7%) and PCL/Gel/C-AgNP(coat) (60.9%) scaffolds. * = $p \leq 0.05$.

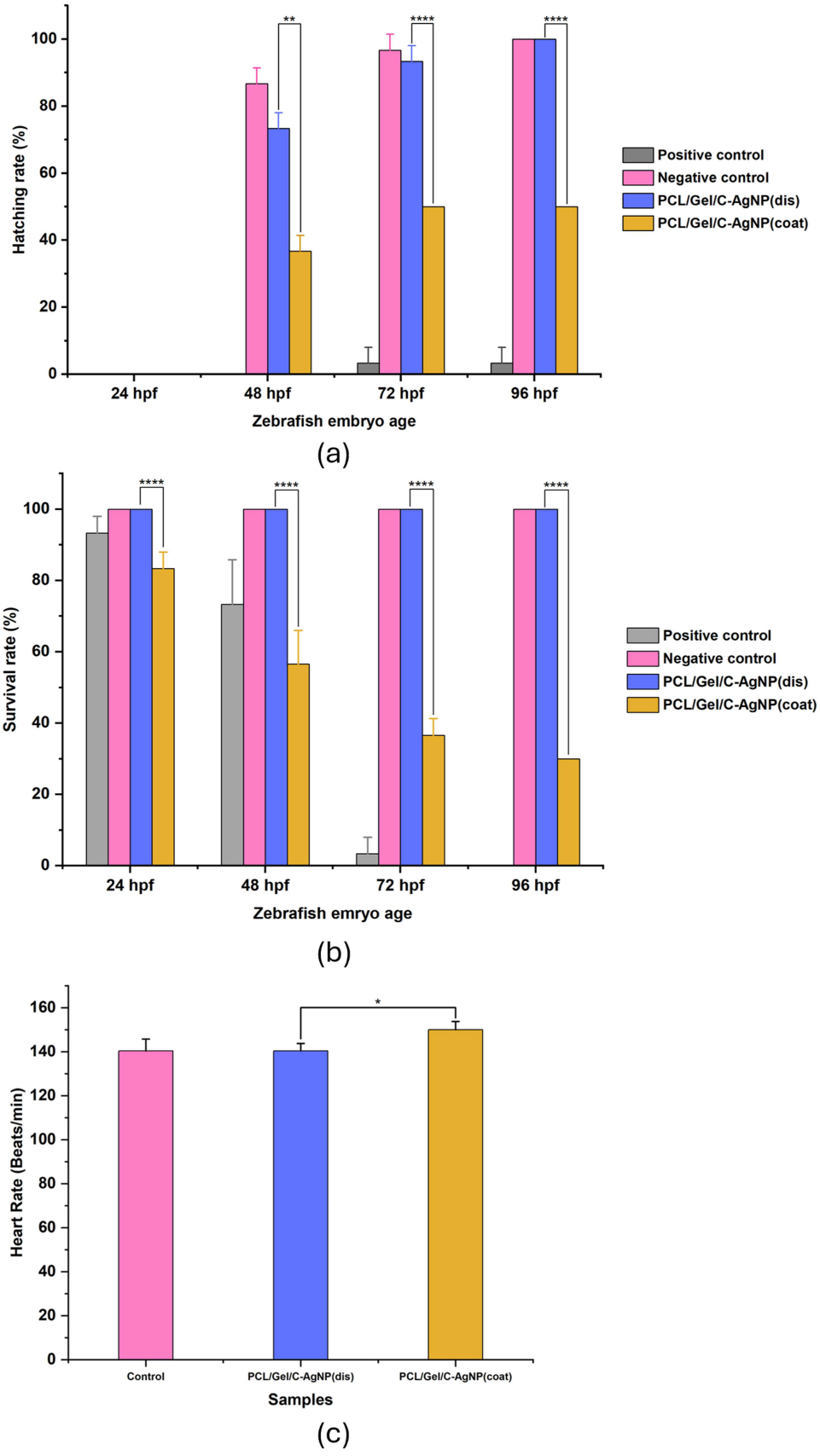

Figure 6. Zebrafish embryo assay results. (a) Hatching rate and (b) survival rate of wild-type zebrafish embryos at 24, 48, 72 and 96 hpf for the PCL/Gel/C-AgNP(dis) and PCL/Gel/C-AgNP(coat) scaffolds. (c) Heart rate (beats/min) of 72 hpf wild-type zebrafish embryos for the PCL/Gel/C-AgNP(dis) and PCL/Gel/C-AgNP(coat) scaffolds as compared to a negative control. * = $p \leq 0.05$, ** = $p \leq 0.01$, *** = $p \leq 0.001$, **** = $p \leq 0.001$.

time point. However, none of the larvae died with either the PCL/Gel/C-AgNP(dis) scaffold treatment and the negative control, which gave a 100% survival rate at all time points. These embryonic cytotoxicity results correlate with the BJ cell viability assay results. However, a significantly lower survival rate for PCL/Gel/C-AgNP(coat) scaffold treatment was observed, suggesting toxicity.

The heart rates were studied in three treatments, the negative control, PCL/Gel/C-AgNP(dis) and PCL/Gel/C-AgNP(coat). These measurements were taken at the 72 hpf time point (Figure 6c). The obtained results showed that there is a significantly higher ($p \leq 0.05$) heart rate for embryos treated with PCL/Gel/C-AgNP(coat) compared to PCL/Gel/C-AgNP(dis), suggesting stress caused by Ag^+ ion release, though the observed rate still lies within the acceptable range [57]. Microscope images of NSD (no structural defects) zebrafish embryos and larvae were recorded, and exemplar digital photographs are shown in the Supporting Information (Figure S4). The three main structural defects, pericardial edimas, yolk sack edimas and spinal curvatures [58], were not observed in embryos treated with either of the scaffolds or the negative control. However, observations of positive control zebrafish indicated that coagulation is the most common form of lethal effect. Considering the hatching rate, survival rate, heart rate and developmental deformities, it can be concluded that the PCL/Gel/C-AgNP(dis) scaffold is not toxic while the PCL/Gel/C-AgNP(coat) system is mildly toxic by the zebrafish toxicity assessment.

Conclusion

This study aimed to investigate the anti-bacterial and toxicity effects of PCL/Gel scaffolds loaded with C-AgNPs either by surface coating [PCL/Gel/C-AgNP(coat)] or via blending to give a homogenous NP distribution throughout the fibres [PCL/Gel/C-AgNP(dis)]. The PCL/Gel/C-AgNP(coat) scaffold demonstrated good antibacterial activity against both *Staphylococcus aureus* and *Escherichia coli* strains, while the PCL/Gel/C-AgNP(dis) scaffold system had no effect. However, PCL/Gel/C-AgNP(coat) showed marked cytotoxicity to healthy BJ human skin fibroblast cells, and also mild toxicity in zebrafish embryonic development assays. In contrast, no toxicity was seen with fibroblasts or zebrafish embryos exposed to PCL/Gel/C-AgNP(dis). Hence, there is a clear trade-off between toxicity and antibacterial efficacy, and the distribution of C-AgNPs in PCL/Gel nanofibers needs to be controlled to ensure that both acceptable antibacterial activity and cytotoxicity can be achieved for skin tissue engineering scaffolds.

Acknowledgements

The authors would like to extend their sincere gratitude to the National Research Council fund (NRC TO 16–18 grant) of the Department of Chemistry of the University of Colombo for the extended support and funding for the research proceedings. We are grateful to all personnel conducting MTT assays at the Institute of Biochemistry, Molecular Biology and Biotechnology (IBMBB). The authors also thank M. K. Gunawardana of the Centre for Advanced Materials and Devices for instrumentation support in XRD analysis. Special appreciation is also provided to M. T. M. R. Jayaweera at the Department of Materials Science & Engineering, Faculty of Engineering, University of Moratuwa, for the instrumentation support supplied in the SEM analysis.

Author contributions

CRediT: Dilshan Chandraguptha: conceptualisation, methodology, formal analysis, data curation, writing-original draft; Lochana Fernando; methodology, formal analysis, data curation, writing-original draft; Lalinka Herath: supervision (zebrafish embryonic toxicity assay), resources; V. Umayangana Godakanda: supervision (electrospinning); Nirmal Perera: methodology (cell proliferation assay); Sameera Samarakoon: resources; K. M. Nalin de Silva: supervision, resources, writing-review and editing; Gareth R. Williams: supervision, resources, writing-review and editing; W. Rohini M. de Silva: conceptualisation, supervision, resources, writing-review and editing. All the authors have read and agreed to the published version of the manuscript.

Disclosure statement

No potential conflict of interest was reported by the author(s).

Data availability statement

The datasets supporting this article will be provided by the corresponding author upon request.

Ethical statement

All zebrafish (*Danio rerio*) protcols were approved for toxicity assessment studies by the Animal Ethics Committee of the Institute of Biology, Sri Lanka (ERC IOBSL 19907 2019). Broodstock maintenance was carried out according to the Organisation for Economic Cooperation and Development (OECD) guideline No. 236 for fish embryo acute toxicity (FET) tests in the mini-zebrafish facility at the Department of Chemistry, University of Colombo, Sri Lanka.

References

[1] Omidian H, Gill E. Nanofibrous scaffolds in biomedicine. J Compos Sci. 2024;8(7):269. doi: 10.3390/jcs8070269
[2] Maran B, Jeyachandran S, Kimura M. A review on the electrospinning of polymer nanofibers and its biomedical applications. J Compos Sci. 2024;8(1):32–32. doi: 10.3390/jcs8010032
[3] Gautam S, Dinda A, Mishra N. Fabrication and characterization of PCL/gelatin composite nanofibrous scaffold for tissue engineering applications by electrospinning method. Mater Sci Eng, C. 2013;33(3):1228–1235. doi: 10.1016/j.msec.2012.12.015
[4] Robles K, Zahra F, Mu R, et al. Advances in electrospun poly(ε-Caprolactone)-based nanofibrous scaffolds for tissue engineering. Polymers. 2024;16(20):2853–2853. doi: 10.3390/polym16202853
[5] Pereira I, Ayres E, Averous L, et al. Differentiation of human adipose-derived stem cells seeded on mineralized electrospun co-axial poly(ε-caprolactone) (PCL)/gelatin nanofibers. J Mater Sci Mater Med. 2014;25(4):1137–1148. doi: 10.1007/s10856-013-5133-9
[6] Borjigin M, Eskridge C, Niamat R, et al. Elessctrospun fiber membranes enable proliferation of genetically modified cells. Int J Nanomedicine. 2013;855–864. doi: 10.2147/IJN.S40117
[7] Yeo M, Kim G. Cell-printed hierarchical scaffolds consisting of micro-sized polycaprolactone (PCL) and electrospun PCL nanofibers/cell-laden alginate struts for tissue regeneration. J Mater Chem B. 2014;2(3):314–324. doi: 10.1039/C3TB21163K
[8] Gautam S, Chou C, Dinda A, et al. Surface modification of nanofibrous polycaprolactone/gelatin composite scaffold by collagen type I grafting for skin tissue engineering. J Mater Sci. 2014;49(3):1076–1089. doi: 10.1007/s10853-013-7785-8
[9] Elango J, Zamora-Ledezma C, Alexis F, et al. Protein adsorption, calcium-binding ability, and biocompatibility of silver nanoparticle-loaded polyvinyl alcohol (PVA) hydrogels using bone marrow-derived mesenchymal stem cells. Pharmaceutics. 2023;15(7):1843–1843. doi: 10.3390/pharmaceutics15071843
[10] Zienkiewicz-Strzałka M, Deryło-Marczewska A, Skorik Y, et al. Silver nanoparticles on Chitosan/Silica nanofibers: characterization and antibacterial activity. Int J Mol Sci. 2019;21(1):166. doi: 10.3390/ijms21010166
[11] Toczek J, Sadłocha M, Major K, et al. Benefit of silver and gold nanoparticles in wound healing process after endometrial cancer protocol. Biomedicines. 2022;10(3):679. doi: 10.3390/biomedicines10030679
[12] Bao H, Yu X, Xu C, et al. New toxicity mechanism of silver nanoparticles: promoting apoptosis and inhibiting proliferation. PLoS One. 2015;10(3):1–10. doi: 10.1371/journal.pone.0122535
[13] Sabarees G, Velmurugan V, Tamilarasi G, et al. Recent advances in silver nanoparticles containing nanofibers for chronic wound management. Polymers (Basel). 2022;14(19):3994. doi: 10.3390/polym14193994
[14] Beyene H, Werkneh A, Bezabh H, et al. Synthesis paradigm and applications of silver nanoparticles (AgNPs), a review. Sustain Mater Technol. 2017;13(January):18–23. doi: 10.1016/j.susmat.2017.08.001
[15] Kalaivani R, Maruthupandy M, Muneeswaran T, et al. Synthesis of chitosan mediated silver nanoparticles (Ag NPs) for potential antimicrobial applications. Front Lab Med. 2018;2(1):30–35. doi: 10.1016/j.flm.2018.04.002
[16] Raafat D, Sahl H. Chitosan and its antimicrobial potential--a critical literature survey. Microb Biotechnol. 2009;2(2 SPEC. ISS.):186–201. doi: 10.1111/j.1751-7915.2008.00080.x
[17] Krishnaraj C, Radhakrishnan S, Ramachandran R, et al. In vitro toxicological assessment and biosensing potential of bioinspired chitosan nanoparticles, selenium nanoparticles, chitosan/selenium nanocomposites, silver nanoparticles and chitosan/silver nanocomposites. Chemosphere. 2022;301(April):134790. doi: 10.1016/j.chemosphere.2022.134790
[18] Samokhin Y, Varava Y, Diedkova K, et al. Electrospun chitosan/polylactic acid nanofibers with silver nanoparticles: structure, antibacterial, and cytotoxic properties. ACS Appl Bio Mater. 2025;8(2):1027–1037. doi: 10.1021/acsabm.4c01252
[19] Torres-Pedroza M, Martínez-Ávila A, Juarez-Moreno K, et al. Multifunctional Biological performance of electrospun pcl scaffolds formulated with silver sulfide nanoparticles. Polymers. 2025;17(2):230–230. doi: 10.3390/polym17020230
[20] Korniienko V, Husak Y, Diedkova K, et al. Antibacterial potential and biocompatibility of chitosan/polycaprolactone nanofibrous membranes incorporated with silver nanoparticles. Polymers. 2024;16(12):1729–1729. doi: 10.3390/polym16121729

[21] Iurilli M, Porrelli D, Turco G, et al. Electrospun collagen-coated nanofiber membranes functionalized with silver nanoparticles for advanced wound healing applications. Membranes. 2025;15(2):39–39. doi: 10.3390/membranes15020039
[22] Kalakonda P, Thudumu S, Mynepall S, et al. Porous micro-/nano-fibrous silver-coated polymeric scaffolds with tunable mechanical properties for wound healing applications. Polym Bull. 2025;82:4443–4457. doi: 10.1007/s00289-025-05672-z
[23] Podgórski R, Wojasiński M, Ciach T. Nanofibrous materials affect the reaction of cytotoxicity assay. Sci Rep. 2022;12(1):1–12. doi: 10.1038/s41598-022-13002-w
[24] Kamiloglu S, Sari G, Ozdal T, et al. Guidelines for cell viability assays. Food Front. 2020;1(3):332–349. doi: 10.1002/fft2.44
[25] Choi T, Choi T, Lee Y, et al. Zebrafish as an animal model for biomedical research. Exp Mol Med. 2021;53(3):310–317. doi: 10.1038/s12276-021-00571-5
[26] Lowery J, Datta N, Rutledge G. Effect of fiber diameter, pore size and seeding method on growth of human dermal fibroblasts in electrospun poly(epsilon-caprolactone) fibrous mats. Biomaterials. 2010;31(3):491–504. doi: 10.1016/j.biomaterials.2009.09.072
[27] Szewczyk K, Pietrzak W, Klimek K, et al. Flavonoid and phenolic acids content and in vitro study of the potential anti-aging properties of *eutrema japonicum* (Miq.) koidz cultivated in wasabi farm Poland. Int J Mol Sci. 2021;22(12):6219. doi: 10.3390/ijms22126219
[28] Unnithan A, Barakat N, Tirupathi Pichiah P, et al. Wound-dressing materials with antibacterial activity from electrospun polyurethane-dextran nanofiber mats containing ciprofloxacin HCl. Carbohydr Polym. 2012;90(4):1786–1793. doi: 10.1016/j.carbpol.2012.07.071
[29] Ediriweera M, Moon J, Nguyen Y, et al. 10-Gingerol targets lipid rafts associated PI3K/Akt signaling in radio-resistant triple negative breast cancer cells. Molecules. 2020;25(14):1–13. doi: 10.3390/molecules25143164
[30] Tudose M, Culita D, Baratoiu-Carpen R, et al. Novel Antitumor agents based on fluorescent benzofurazan derivatives and mesoporous silica. Int J Mol Sci. 2022;23(24):15663. doi: 10.3390/ijms232415663
[31] Sobanska M, Scholz S, Nyman A, et al. Applicability of the fish embryo acute toxicity (FET) test (OECD 236) in the regulatory context of registration, evaluation, authorisation, and restriction of chemicals (REACH). Environ Toxicol Chem. 2018;37(3):657–670. doi: 10.1002/etc.4055
[32] Sadasivam R, Mohiyuddin S, Packirisamy G. Electrospun polyacrylonitrile (PAN) templated 2D Nanofibrous mats: a platform toward practical applications for dye removal and bacterial disinfection. ACS Omega. 2017;2(10):6556–6569. doi: 10.1021/acsomega.7b01101
[33] Mendis J, Tennakoon T, Jayasinghe C. Zebrafish embryo toxicity of a binary mixture of pyrethroid insecticides: d-tetramethrin and cyphenothrin. J Toxicol. 2018;2018:1–8. doi: 10.1155/2018/4182694
[34] Keast V. Atmospheric corrosion of silver and silver nanoparticles. Corros Mater Degrad. 2022;3(2):221–234. doi: 10.3390/cmd3020013
[35] Mulvaney P. Surface plasmon spectroscopy of nanosized metal particles. Langmuir. 1996;12(3):788–800. doi: doi/10.1021/la9502711
[36] Darroudi M, Ahmad M, Abdullah A, et al. Effect of accelerator in green synthesis of silver nanoparticles. Int J Mol Sci. 2010;11(10):3898–3905. doi: 10.3390/ijms11103898
[37] Alqadi M, Abo Noqtah O, Alzoubi J, et al. Polycaprolactone (PCL) Chains grafting on the surface of cellulose nanocrystals (CNCs) during In Situ Polymerization of ε-caprolactone at room temperature. Mater Sci Pol. 2014;32(1):107–111. doi: 10.4236/msa.2020.1111050
[38] Wang S, Zhao Y, Shen M, et al. Electrospun hybrid nanofibers doped with nanoparticles or nanotubes for biomedical applications. Ther Deliv. 2012;3(10):1155–1169. doi: 10.4155/tde.12.103
[39] Merkle V, Tran P, Hutchinson M, et al. Core-shell PVA/gelatin electrospun nanofibers promote human umbilical vein endothelial cell and smooth muscle cell proliferation and migration. Acta Biomater. 2015;27:77–87. doi: 10.1016/j.actbio.2015.08.044
[40] Katsogiannis K, Vladisavljević G, Georgiadou S. Porous electrospun polycaprolactone (PCL) fibres by phase separation. Eur Polym J. 2015;69:284–295. doi: 10.1016/j.eurpolymj.2015.01.028
[41] Zhang Q, Lv S, Lu J, et al. Characterization of polycaprolactone/collagen fibrous scaffolds by electrospinning and their bioactivity. Int J Biol Macromol. 2015;76:94–101. doi: 10.1016/j.ijbiomac.2015.01.063
[42] Kuppan P, Sethuraman S, Krishnan U. PCL and PCL-gelatin nanofibers as esophageal tissue scaffolds: optimization, characterization and cell-matrix interactions. J Biomed Nanotechnol. 2013;9(9):1540–1555. doi: 10.1166/jbn.2013.1653
[43] Rahma A, Munir M, Khairurrijal Prasetyo A, et al. Intermolecular interactions and the release pattern of electrospun curcumin-polyvinyl(pyrrolidone) Fiber. Biol Pharm Bull. 2016;39(2):163–173. doi: 10.1248/bpb.b15-00391
[44] Anees Ahmad S, Sachi Das S, Khatoon A, et al. Bactericidal activity of silver nanoparticles: a mechanistic review. Mater Sci Energy Technol. 2020;3:756–769. doi: 10.1016/j.mset.2020.09.002
[45] Bruna T, Maldonado-Bravo F, Jara P, et al. Silver nanoparticles and their antibacterial applications. Int J Mol Sci. 2021;22(13):7202. doi: 10.3390/ijms22137202

[46] Yin IX, Zhang J, Zhao IS, et al. The antibacterial mechanism of silver nanoparticles and its application in dentistry. Int J Nanomedicine. 2020;15:2555–2562. doi: 10.2147/IJN.S246764
[47] Mikhailova E. Silver nanoparticles: mechanism of action and probable bio-application. J Funct Biomater. 2020;11(4):84. doi: 10.3390/jfb11040084
[48] Wilhelm M, Gh., Sharifian M, Wu T, et al. Determination of bacterial surface charge density via saturation of adsorbed ions. Biophys J. 2021;120(12):2461–2470. doi: 10.1016/j.bpj.2021.04.018
[49] Zhang T, Wang L, Chen Q, et al. Cytotoxic potential of silver nanoparticles. Yonsei Med J. 2014;55(2):283–291. doi: 10.3349/ymj.2014.55.2.283
[50] Akter M, Sikder M, Rahman M, et al. A systematic review on silver nanoparticles-induced cytotoxicity: physicochemical properties and perspectives. J Adv Res. 2018;9:1–16. doi: 10.1016/j.jare.2017.10.008
[51] Teame T, Zhang Z, Ran C, et al. The use of zebrafish (*Danio rerio*) as biomedical models. Anim Front. 2019;9(3):68–77. doi: 10.1093/af/vfz020
[52] Veldman M, Lin S. Zebrafish as a developmental model organism for pediatric research. Pediatr Res. 2008;64(5):470–476. doi: 10.1203/PDR.0b013e318186e609
[53] Siddiqui S, Siddiqui H, Riguene E, et al. Zebrafish: A versatile and powerful model for biomedical research. BioEssays. 2025;e70080. doi: 10.1002/bies.70080
[54] Saleem S, Kannan RR. Zebrafish: An emerging real-time model system to study Alzheimer's disease and neurospecific drug discovery. Cell Death Discov. 2018;4(1):45. doi: 10.1038/s41420-018-0109-7
[55] Adhish M, Manjubala I. Effectiveness of zebrafish models in understanding human diseases-a review of models. Heliyon. 2023;9(3):e14557. doi: 10.1016/j.heliyon.2023.e14557
[56] Vimalraj S, Yuvashree R, Hariprabu G, et al. Zebrafish as a potential biomaterial testing platform for bone tissue engineering application: a special note on chitosan-based bioactive materials. Int J Biol Macromol. 2021; 175:379–395. doi: 10.1016/j.ijbiomac.2021.02.005
[57] De Luca E, Zaccaria G, Hadhoud M, et al. *ZebraBeat*: a flexible platform for the analysis of the cardiac rate in zebrafish embryo. Sci Rep. 2014;4:1–13.
[58] Schwartz A, Sant K, George U. Development of a dynamic network model to identify temporal patterns of structural malformations in zebrafish embryos exposed to a model toxicant, tris(4-chlorophenyl)methanol. J Xenobiot. 2023;13(2):284–297. doi: 10.3390/jox13020021